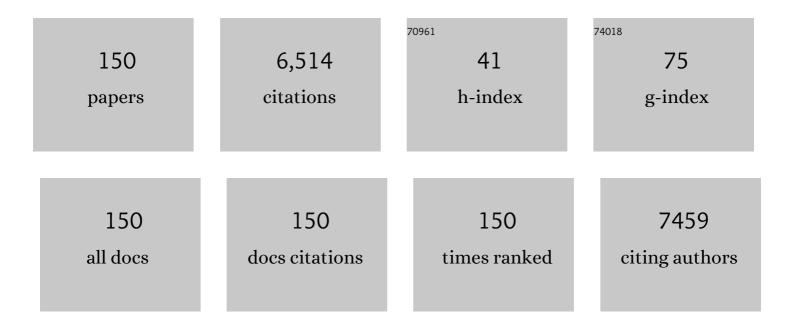
Min-Ying Su

List of Publications by Year in descending order

Source: https://exaly.com/author-pdf/3865136/publications.pdf Version: 2024-02-01



#	Article	IF	CITATIONS
1	Editorial for "Radiomicâ€Based MRI for Classification of Solitary Brain Metastasis Subtypes From Primary Lymphoma of the Central Nervous Systemâ€: Journal of Magnetic Resonance Imaging, 2023, 57, 236-237.	1.9	0
2	Automatic Detection and Segmentation of Breast Cancer on MRI Using Mask R-CNN Trained on Non–Fat-Sat Images and Tested on Fat-Sat Images. Academic Radiology, 2022, 29, S135-S144.	1.3	33
3	Multiâ€parametric MRI (mpMRI) for treatment response assessment of radiation therapy. Medical Physics, 2022, 49, 2794-2819.	1.6	3
4	Usage of image registration and three-dimensional visualization tools on serial computed tomography for the analysis of patients with traumatic intraparenchymal hemorrhages. Journal of Clinical Neuroscience, 2022, 98, 154-161.	0.8	0
5	Prediction of Intraparenchymal Hemorrhage Progression and Neurologic Outcome in Traumatic Brain Injury Patients Using Radiomics Score and Clinical Parameters. Diagnostics, 2022, 12, 1677.	1.3	7
6	Prediction of breast cancer molecular subtypes on DCE-MRI using convolutional neural network with transfer learning between two centers. European Radiology, 2021, 31, 2559-2567.	2.3	67
7	Improving CBCT quality to CT level using deep learning with generative adversarial network. Medical Physics, 2021, 48, 2816-2826.	1.6	64
8	Editorial for "The Occurrence and Outcome of Mild Intracranial Atherosclerotic Stenosis: A Prospective <scp>Highâ€Resolution MRI</scp> Study― Journal of Magnetic Resonance Imaging, 2021, 54, 89-90.	1.9	0
9	Prediction of the early recurrence in spinal giant cell tumor of bone using radiomics of preoperative CT: Long-term outcome of 62 consecutive patients. Journal of Bone Oncology, 2021, 27, 100354.	1.0	14
10	Differential diagnosis of benign and malignant vertebral fracture on CT using deep learning. European Radiology, 2021, 31, 9612-9619.	2.3	28
11	Pre-operative MRI Radiomics for the Prediction of Progression and Recurrence in Meningiomas. Frontiers in Neurology, 2021, 12, 636235.	1.1	22
12	Development of U-Net Breast Density Segmentation Method for Fat-Sat MR Images Using Transfer Learning Based on Non-Fat-Sat Model. Journal of Digital Imaging, 2021, 34, 877-887.	1.6	11
13	BI-RADS Reading of Non-Mass Lesions on DCE-MRI and Differential Diagnosis Performed by Radiomics and Deep Learning. Frontiers in Oncology, 2021, 11, 728224.	1.3	7
14	Diagnosis of Breast Cancer Using Radiomics Models Built Based on Dynamic Contrast Enhanced MRI Combined With Mammography. Frontiers in Oncology, 2021, 11, 774248.	1.3	3
15	Clinical Significance of Preoperative CT and MR Imaging Findings in the Prediction of Postoperative Recurrence of Spinal Giant Cell Tumor of Bone. Orthopaedic Surgery, 2021, 13, 2405-2416.	0.7	1
16	Diagnosis of Benign and Malignant Breast Lesions on DCEâ€MRI by Using Radiomics and Deep Learning With Consideration of Peritumor Tissue. Journal of Magnetic Resonance Imaging, 2020, 51, 798-809.	1.9	125
17	Diagnosis of spinal lesions using perfusion parameters measured by DCE-MRI and metabolism parameters measured by PET/CT. European Spine Journal, 2020, 29, 1061-1070.	1.0	3
18	Quantitative assessment of breast density using transmission ultrasound: comparison to MRI-based		0

breast density. , 2020, , .

#	Article	IF	CITATIONS
19	Radiomics approach for prediction of recurrence in skull base meningiomas. Neuroradiology, 2019, 61, 1355-1364.	1.1	46
20	Combinatorial targeting of cancer bone metastasis using mRNA engineered stem cells. EBioMedicine, 2019, 45, 39-57.	2.7	18
21	Evaluation of breast stiffness measured by ultrasound and breast density measured by MRI using a prone-supine deformation model. Biomarker Research, 2019, 7, 20.	2.8	14
22	Automatic Breast and Fibroglandular Tissue Segmentation in Breast MRI Using Deep Learning by a Fully-Convolutional Residual Neural Network U-Net. Academic Radiology, 2019, 26, 1526-1535.	1.3	70
23	Machine learning for prediction of chemoradiation therapy response in rectal cancer using pre-treatment and mid-radiation multi-parametric MRI. Magnetic Resonance Imaging, 2019, 61, 33-40.	1.0	83
24	Differentiation of spinal metastases originated from lung and other cancers using radiomics and deep learning based on DCE-MRI. Magnetic Resonance Imaging, 2019, 64, 4-12.	1.0	64
25	Feasibility and Diagnostic Performance of Voxelwise Computed Diffusionâ€Weighted Imaging in Breast Cancer. Journal of Magnetic Resonance Imaging, 2019, 49, 1610-1616.	1.9	13
26	Automatic and fast segmentation of breast region-of-interest (ROI) and density in MRIs. Heliyon, 2018, 4, e01042.	1.4	31
27	An image segmentation framework for extracting tumors from breast magnetic resonance images. Journal of Innovative Optical Health Sciences, 2018, 11, .	0.5	17
28	Quantitative analysis of peri-tumor fat in different molecular subtypes of breast cancer. Magnetic Resonance Imaging, 2018, 53, 34-39.	1.0	9
29	Role of dynamic contrastâ€enhanced MRI in evaluating the association between contralateral parenchymal enhancement and survival outcome in ERâ€positive, HER2â€negative, nodeâ€negative invasive breast cancer. Journal of Magnetic Resonance Imaging, 2018, 48, 1678-1689.	1.9	16
30	Deep-Learning Convolutional Neural Networks Accurately Classify Genetic Mutations in Gliomas. American Journal of Neuroradiology, 2018, 39, 1201-1207.	1.2	323
31	Hybrid 3D/2D Convolutional Neural Network for Hemorrhage Evaluation on Head CT. American Journal of Neuroradiology, 2018, 39, 1609-1616.	1.2	183
32	3D MRI for Quantitative Analysis of Quadrant Percent Breast Density. Academic Radiology, 2017, 24, 811-817.	1.3	4
33	Diagnosis of Spinal Lesions Using Heuristic and Pharmacokinetic Parameters Measured by Dynamic Contrast-Enhanced MRI. Academic Radiology, 2017, 24, 867-875.	1.3	11
34	Evaluation of the association between quantitative mammographic density and breast cancer occurred in different quadrants. BMC Cancer, 2017, 17, 274.	1.1	22
35	A multi-resolution approach for spinal metastasis detection using deep Siamese neural networks. Computers in Biology and Medicine, 2017, 84, 137-146.	3.9	96
36	Hypothermic Cooling Measured by Thermal Magnetic Resonance Imaging; Feasibility and Implications for Virtual Imaging in the Urogenital Pelvis. Urology, 2017, 108, 220-224.	0.5	4

#	Article	IF	CITATIONS
37	Sample size and power determination when limited preliminary information is available. BMC Medical Research Methodology, 2017, 17, 75.	1.4	6
38	Morphological and dynamic contrast enhanced MR imaging features for the differentiation of chordoma and giant cell tumors in the Axial Skeleton. Journal of Magnetic Resonance Imaging, 2017, 45, 1068-1075.	1.9	20
39	Breast density quantification using structured-light-based diffuse optical tomography simulations. Applied Optics, 2017, 56, 7146.	0.9	15
40	Impact of Different Analytic Approaches on the Analysis of the Breast Fibroglandular Tissue Using Diffusion Weighted Imaging. BioMed Research International, 2017, 2017, 1-11.	0.9	3
41	Tensor based multichannel reconstruction for breast tumours identification from DCE-MRIs. PLoS ONE, 2017, 12, e0172111.	1.1	13
42	US-localized diffuse optical tomography in breast cancer: comparison with pharmacokinetic parameters of DCE-MRI and with pathologic biomarkers. BMC Cancer, 2016, 16, 50.	1.1	9
43	Opportunistic Breast Density Assessment in Women Receiving Low-dose Chest Computed Tomography Screening. Academic Radiology, 2016, 23, 1154-1161.	1.3	10
44	Pattern identification of biomedical images with time series: Contrasting THz pulse imaging with DCE-MRIs. Artificial Intelligence in Medicine, 2016, 67, 1-23.	3.8	19
45	Diffuse optical tomography with structured-light patterns to quantify breast density. Proceedings of SPIE, 2016, , .	0.8	0
46	Imaging Breast Density: Established and Emerging Modalities. Translational Oncology, 2015, 8, 435-445.	1.7	25
47	Quantification of Regional Breast Density in Four Quadrants Using 3D MRI—A Pilot Study. Translational Oncology, 2015, 8, 250-257.	1.7	5
48	Investigation of factors affecting hypothermic pelvic tissue cooling using bio-heat simulation based on MRI-segmented anatomic models. Computer Methods and Programs in Biomedicine, 2015, 122, 76-88.	2.6	6
49	Differentiation of tuberculosis and metastatic cancer in the spine using dynamic contrast-enhanced MRI. European Spine Journal, 2015, 24, 1729-1737.	1.0	34
50	Impact of positional difference on the measurement of breast density using MRI. Medical Physics, 2015, 42, 2268-2275.	1.6	6
51	Double-Blind Randomized 12-Month Soy Intervention Had No Effects on Breast MRI Fibroglandular Tissue Density or Mammographic Density. Cancer Prevention Research, 2015, 8, 942-951.	0.7	32
52	Background Parenchymal Enhancement of the Contralateral Normal Breast: Association with Tumor Response in Breast Cancer Patients Receiving Neoadjuvant Chemotherapy. Translational Oncology, 2015, 8, 204-209.	1.7	53
53	Long-term Follow-up of Breast-conserving Therapy in Patients with Inflammatory Breast Cancer Treated with Neoadjuvant Chemotherapy. American Surgeon, 2014, 80, 940-943.	0.4	24
54	Impact of factors affecting the residual tumor size diagnosed by MRI following neoadjuvant chemotherapy in comparison to pathology. Journal of Surgical Oncology, 2014, 109, 158-167.	0.8	43

Min-Ying Su

#	Article	IF	CITATIONS
55	Long-term follow-up of breast-conserving therapy in patients with inflammatory breast cancer treated with neoadjuvant chemotherapy. American Surgeon, 2014, 80, 940-3.	0.4	14
56	Optical imaging correlates with magnetic resonance imaging breast density and revealscomposition changes during neoadjuvant chemotherapy. Breast Cancer Research, 2013, 15, R14.	2.2	56
57	Specificity enhancement in classification of breast MRI lesion based on multi-classifier. Neural Computing and Applications, 2013, 22, 35-45.	3.2	12
58	Developmental changes in hippocampal shape among preadolescent children. International Journal of Developmental Neuroscience, 2013, 31, 473-481.	0.7	23
59	Templateâ€based automatic breast segmentation on MRI by excluding the chest region. Medical Physics, 2013, 40, 122301.	1.6	51
60	Differentiation of myeloma and metastatic cancer in the spine using dynamic contrast-enhanced MRI. Magnetic Resonance Imaging, 2013, 31, 1285-1291.	1.0	37
61	Effect of taxaneâ€based neoadjuvant chemotherapy on fibroglandular tissue volume and percent breast density in the contralateral normal breast evaluated by 3T MR. NMR in Biomedicine, 2013, 26, 1705-1713.	1.6	9
62	Early Clinical PET Imaging Results with the Novel PHF-Tau Radioligand [F-18]-T807. Journal of Alzheimer's Disease, 2013, 34, 457-468.	1.2	598
63	Background parenchymal enhancement in the contralateral normal breast of patients undergoing neoadjuvant chemotherapy measured by DCE-MRI. Magnetic Resonance Imaging, 2013, 31, 1465-1471.	1.0	31
64	Response of bilateral breasts to the endogenous hormonal fluctuation in a menstrual cycle evaluated using 3D MRI. Magnetic Resonance Imaging, 2013, 31, 538-544.	1.0	18
65	Clinical Application of Magnetic Resonance Imaging in Management of Breast Cancer Patients Receiving Neoadjuvant Chemotherapy. BioMed Research International, 2013, 2013, 1-14.	0.9	20
66	Correlation of endogenous hormonal levels, fibroglandular tissue volume and percent density measured using 3D MRI during one menstrual cycle. Annals of Oncology, 2013, 24, 2329-2335.	0.6	14
67	Breast density quantification using magnetic resonance imaging (MRI) with bias field correction: A postmortem study. Medical Physics, 2013, 40, 122305.	1.6	11
68	Early Clinical PET Imaging Results with the Novel PHF-Tau Radioligand [F18]-T808. Journal of Alzheimer's Disease, 2013, 38, 171-184.	1.2	418
69	Diagnostic Performance of Magnetic Resonance Imaging for Assessing Tumor Response in Patients With HER2-Negative Breast Cancer Receiving Neoadjuvant Chemotherapy is Associated With Molecular Biomarker Profile. Clinical Breast Cancer, 2012, 12, 110-118.	1.1	36
70	Development of white matter pathways in typically developing preadolescent children. Brain Research, 2012, 1466, 33-43.	1.1	30
71	Consistency of breast density measured from the same women in four different MR scanners. Medical Physics, 2012, 39, 4886-4895.	1.6	8
72	A new bias field correction method combining N3 and FCM for improved segmentation of breast density on MRI. Medical Physics, 2011, 38, 5-14.	1.6	52

#	Article	IF	CITATIONS
73	Comparison of breast density measured on MR images acquired using fatâ€suppressed versus nonfatâ€suppressed sequences. Medical Physics, 2011, 38, 5961-5968.	1.6	28
74	Clinical characteristics and biomarkers of breast cancer associated with choline concentration measured by ¹ H MRS. NMR in Biomedicine, 2011, 24, 316-324.	1.6	48
75	<i>In vivo</i> ¹ H MRS in the assessment of the therapeutic response of breast cancer patients. NMR in Biomedicine, 2011, 24, 700-711.	1.6	41
76	Reduction of breast density following tamoxifen treatment evaluated by 3-D MRI: preliminary study. Magnetic Resonance Imaging, 2011, 29, 91-98.	1.0	36
77	Spatial shrinkage/expansion patterns between breast density measured in two MRI scans evaluated by non-rigid registration. Physics in Medicine and Biology, 2011, 56, 5865-5875.	1.6	6
78	Breast Cancer: Evaluation of Response to Neoadjuvant Chemotherapy with 3.0-T MR Imaging. Radiology, 2011, 261, 735-743.	3.6	63
79	Menstrual Cycle–related Fluctuations in Breast Density Measured by Using Three-dimensional MR Imaging. Radiology, 2011, 261, 744-751.	3.6	34
80	Angiogenesis in the Progression of Breast Ductal Proliferations. International Journal of Surgical Pathology, 2011, 19, 335-341.	0.4	20
81	Impact of skin removal on quantitative measurement of breast density using MRI. Medical Physics, 2010, 37, 227-233.	1.6	18
82	Quantitative analysis of breast parenchymal patterns using 3D fibroglandular tissues segmented based on MRI. Medical Physics, 2010, 37, 217-226.	1.6	31
83	Age―and raceâ€dependence of the fibroglandular breast density analyzed on 3D MRI. Medical Physics, 2010, 37, 2770-2776.	1.6	37
84	Continued Exploration of Bevacizumab in Breast Cancer. Annals of Surgical Oncology, 2010, 17, 655-656.	0.7	0
85	Magnetic Resonance Imaging Evaluation of Noninflammatory Breast Cancer with Skin Involvement After Neoadjuvant Chemotherapy. Annals of Surgical Oncology, 2010, 17, 1964-1965.	0.7	0
86	Selection of diagnostic features on breast MRI to differentiate between malignant and benign lesions using computer-aided diagnosis: differences in lesions presenting as mass and non-mass-like enhancement. European Radiology, 2010, 20, 771-781.	2.3	126
87	Characterization of Pure Ductal Carcinoma In Situ on Dynamic Contrast-Enhanced MR Imaging: Do Nonhigh Grade and High Grade Show Different Imaging Features?. Journal of Oncology, 2010, 2010, 1-9.	0.6	35
88	Decrease in Breast Density in the Contralateral Normal Breast of Patients Receiving Neoadjuvant Chemotherapy: MR Imaging Evaluation. Radiology, 2010, 255, 44-52.	3.6	37
89	Foreword. Technology in Cancer Research and Treatment, 2010, 9, 1-3.	0.8	0
90	Can proton MRS provide useful information for characterizing estrogen receptor status in breast cancer?. Annals of Oncology, 2010, 21, 663-665.	0.6	0

#	Article	IF	CITATIONS
91	Computational simulation of breast compression based on segmented breast and fibroglandular tissues on magnetic resonance images. Physics in Medicine and Biology, 2010, 55, 4153-4168.	1.6	34
92	Alterations in Regional Brain Volume and Individual MRI-Guided Perfusion in Normal Control, Stable Mild Cognitive Impairment, and MCI-AD Converter. Journal of Geriatric Psychiatry and Neurology, 2009, 22, 35-45.	1.2	22
93	Comparison of breast density in the contralateral normal breast of patients with invasive and in situ breast cancer measured on MRI. Annals of Oncology, 2009, 20, 1449-1450.	0.6	1
94	Predicting Pathologic Response to Neoadjuvant Chemotherapy in Breast Cancer by Using MR Imaging and Quantitative ¹ H MR Spectroscopy. Radiology, 2009, 251, 653-662.	3.6	128
95	Does breast density show difference in patients with estrogen receptor-positive and estrogen receptor-negative breast cancer measured on MRI?. Annals of Oncology, 2009, 20, 1447-1449.	0.6	15
96	Algorithmâ€based method for detection of blood vessels in breast MRI for development of computerâ€aided diagnosis. Journal of Magnetic Resonance Imaging, 2009, 30, 817-824.	1.9	15
97	Residual Breast Cancer Diagnosed by MRI in Patients Receiving Neoadjuvant Chemotherapy with and Without Bevacizumab. Annals of Surgical Oncology, 2009, 16, 1619-1628.	0.7	70
98	Prediction of Malignant Breast Lesions from MRI Features. Academic Radiology, 2009, 16, 842-851.	1.3	74
99	Impact of MRI-Evaluated Neoadjuvant Chemotherapy Response on Change of Surgical Recommendation in Breast Cancer. Annals of Surgery, 2009, 249, 448-454.	2.1	45
100	Fibrocystic change of the breast presenting as a focal lesion mimicking breast cancer in MR imaging. Journal of Magnetic Resonance Imaging, 2008, 28, 1499-1505.	1.9	43
101	Quantitative correlation between 1H MRS and dynamic contrast-enhanced MRI of human breast cancer. Magnetic Resonance Imaging, 2008, 26, 523-531.	1.0	34
102	Magnetic resonance imaging features of fibrocystic change of the breast. Magnetic Resonance Imaging, 2008, 26, 1207-1214.	1.0	34
103	Pathological Axillary Lymph Node Status in HER-2 Receptor Positive and Negative Breast Cancers. Annals of Surgical Oncology, 2008, 15, 941-942.	0.7	1
104	Inflammatory Breast Cancer After Neoadjuvant Chemotherapy: Can Magnetic Resonance Imaging Precisely Diagnose the Final Pathological Response?. Annals of Surgical Oncology, 2008, 15, 3609-3613.	0.7	15
105	Quantitative Analysis of Lesion Morphology and Texture Features for Diagnostic Prediction in Breast MRI. Academic Radiology, 2008, 15, 1513-1525.	1.3	207
106	Can dynamic contrast-enhanced MRI (DCE-MRI) predict tumor recurrence and lymph node status in patients with breast cancer?. Annals of Oncology, 2008, 19, 822-824.	0.6	19
107	MR imaging features of invasive breast cancer correlated with hormonal receptors: does progesterone receptor matter?. Annals of Oncology, 2008, 19, 1024-1025.	0.6	3
108	Proton MR spectroscopy for monitoring early treatment response of breast cancer to neo-adjuvant chemotherapy. Annals of Oncology, 2008, 19, 1022-1024.	0.6	42

#	Article	IF	CITATIONS
109	Development of a quantitative method for analysis of breast density based on threeâ€dimensional breast MRI. Medical Physics, 2008, 35, 5253-5262.	1.6	155
110	Behavioral, Histological, and Ex Vivo Magnetic Resonance Imaging Assessment of Graded Contusion Spinal Cord Injury in Mice. Journal of Neurotrauma, 2007, 24, 674-689.	1.7	66
111	MRI features of breast cancer: a correlation study with HER-2 receptor. Annals of Oncology, 2007, 18, 1903-1904.	0.6	18
112	Magnetic Resonance Imaging in Predicting Pathological Response of Triple Negative Breast Cancer Following Neoadjuvant Chemotherapy. Journal of Clinical Oncology, 2007, 25, 5667-5669.	0.8	24
113	Triple-negative breast cancer: MRI features in 29 patients. Annals of Oncology, 2007, 18, 2042-2043.	0.6	66
114	Pathological Complete Response in Triple Negative Poorly Differentiated Invasive Ductal Breast Carcinoma Detected During Pregnancy. Journal of Clinical Oncology, 2007, 25, 2618-2620.	0.8	10
115	Breast Delineation using Active Contours to Facilitate Coregistration of Serial MRI Studies for Therapy Response Evaluation. , 2007, , .		3
116	The Predictive Value of Sentinel Lymph Node Biopsy in Locally Advanced Breast Cancer Patients who Have Undergone Neoadjuvant Chemotherapy. American Surgeon, 2007, 73, 977-980.	0.4	11
117	MRI measurements of tumor size and pharmacokinetic parameters as early predictors of response in breast cancer patients undergoing neoadjuvant anthracycline chemotherapy. Journal of Magnetic Resonance Imaging, 2007, 26, 615-623.	1.9	77
118	Application of an automated voxel-based morphometry technique to assess regional gray and white matter brain atrophy in a canine model of aging. NeuroImage, 2006, 29, 234-244.	2.1	56
119	Quantification of Choline-containing Compounds in Malignant Breast Tumors by 1H MR Spectroscopy Using Water as an Internal Reference at 1.5ÂT. Magnetic Resonance Materials in Physics, Biology, and Medicine, 2006, 19, 96-104.	1.1	81
120	Vascular volume and blood-brain barrier permeability measured by dynamic contrast enhanced MRI in hippocampus and cerebellum of patients with MCI and normal controls. Journal of Magnetic Resonance Imaging, 2006, 24, 695-700.	1.9	81
121	Resolution Improvement in Positron Emission Tomography Using Anatomical Magnetic Resonance Imaging. Technology in Cancer Research and Treatment, 2006, 5, 311-317.	0.8	3
122	Regional Pattern of Increased Water Diffusivity in Hippocampus and Corpus Callosum in Mild Cognitive Impairment. Dementia and Geriatric Cognitive Disorders, 2006, 22, 223-229.	0.7	22
123	Regional Quantification of White Matter Hyperintensity in Normal Aging, Mild Cognitive Impairment, and Alzheimer's Disease. Dementia and Geriatric Cognitive Disorders, 2006, 22, 177-184.	0.7	41
124	Comparison of choline and pharmacokinetic parameters in breast cancer measured by MR spectroscopic imaging and dynamic contrast enhanced MRI. Technology in Cancer Research and Treatment, 2006, 5, 401-10.	0.8	20
125	Coregistration of Dynamic Contrast Enhanced MRI and Broadband Diffuse Optical Spectroscopy for Characterizing Breast Cancer. Technology in Cancer Research and Treatment, 2005, 4, 549-558.	0.8	29
126	Pharmacokinetic Parameters Analyzed from MR Contrast Enhancement Kinetics of Multiple Malignant and Benign Breast Lesions Detected in the Same Patients. Technology in Cancer Research and Treatment, 2005, 4, 255-263.	0.8	15

#	Article	IF	CITATIONS
127	A longitudinal study of brain morphometrics using serial magnetic resonance imaging analysis in a canine model of aging. Progress in Neuro-Psychopharmacology and Biological Psychiatry, 2005, 29, 389-397.	2.5	56
128	Effects of scopolamine challenge on regional cerebral blood volume. A pharmacological model to validate the use of contrast enhanced magnetic resonance imaging to assess cerebral blood volume in a canine model of aging. Progress in Neuro-Psychopharmacology and Biological Psychiatry, 2005, 29, 399-406.	2.5	14
129	Frontal Lobe Volume, Function, and Â-Amyloid Pathology in a Canine Model of Aging. Journal of Neuroscience, 2004, 24, 8205-8213.	1.7	135
130	Increased Blood Clotting, Microvascular Density, and Inflammation in Eotaxin-Secreting Tumors Implanted into Mice. American Journal of Pathology, 2004, 165, 449-456.	1.9	13
131	Monitoring the Size and Response of Locally Advanced Breast Cancers to Neoadjuvant Chemotherapy (Weekly Paclitaxel and Epirubicin) with Serial Enhanced MRI. Breast Cancer Research and Treatment, 2003, 78, 51-58.	1.1	131
132	Correlation of dynamic contrast enhancement MRI parameters with microvessel density and VEGF for assessment of angiogenesis in breast cancer. Journal of Magnetic Resonance Imaging, 2003, 18, 467-477.	1.9	150
133	Inhibition of thrombosis in melanoma allografts in mice by endogenous mast cell heparin. Thrombosis and Haemostasis, 2003, 90, 351-360.	1.8	14
134	Applications of Dynamic Contrast Enhanced MRI in Oncology: Measurement of Tumor Oxygen Tension. Technology in Cancer Research and Treatment, 2002, 1, 29-38.	0.8	21
135	Measurement of Volumetric and Vascular Changes with Dynamic Contrast Enhanced MRI for Cancer Therapy Monitoring. Technology in Cancer Research and Treatment, 2002, 1, 479-488.	0.8	9
136	Lumpy silicone-injected breasts. Clinical Imaging, 2002, 26, 397-404.	0.8	31
137	Assessment of protamine-induced thrombosis of tumor vessels for cancer therapy using dynamic contrast-enhanced MRI. NMR in Biomedicine, 2002, 15, 106-113.	1.6	15
138	Selective Thrombosis of Tumor Blood Vessels in Mammary Adenocarcinoma Implants in Rats. American Journal of Pathology, 2001, 159, 245-251.	1.9	13
139	Effect of vasodilator hydralazine on tumor microvascular random flow and blood volume as measured by intravoxel incoherent motion (IVIM) weighted MRI in conjunction with Gd-DTPA-Albumin enhanced MRI. Magnetic Resonance Imaging, 2001, 19, 1063-1072.	1.0	18
140	Prediction of gene therapy-induced tumor size changes by the vascularity changes measured using dynamic contrast-enhanced MRIâ~†. Magnetic Resonance Imaging, 2000, 18, 311-317.	1.0	20
141	Investigation of longitudinal vascular changes in control and chemotherapy-treated tumors to serve as therapeutic efficacy predictors. Journal of Magnetic Resonance Imaging, 1999, 9, 128-137.	1.9	34
142	Characterization of N-ethyl-N-nitrosourea-induced malignant and benign breast tumors in rats by using three MR contrast agents. Journal of Magnetic Resonance Imaging, 1999, 9, 177-186.	1.9	57
143	Tumor characterization with dynamic contrast–enhanced MRI using mr contrast agents of various molecular weights. Magnetic Resonance in Medicine, 1998, 39, 259-269.	1.9	140
144	Measurement of tumor vascular volume and mean microvascular random flow velocity magnitude by dynamic GD-DTPA-Albumin enhanced and diffusion-weighted MRI. Magnetic Resonance in Medicine, 1998, 40, 397-404.	1.9	17

#	Article	IF	CITATIONS
145	Magnetic resonance imaging of anatomic and vascular characteristics in a canine model of human aging. Neurobiology of Aging, 1998, 19, 479-485.	1.5	116
146	Pharmacokinetic changes induced by vasomodulators in kidneys, livers, muscles, and implanted tumors in rats as measured by dynamic Gd-DTPA-enhanced MRI. Magnetic Resonance in Medicine, 1996, 36, 868-877.	1.9	19
147	Regional comparison of tumor vascularity and permeability parameters measured by albumin-GD-DTPA and GD-DTPA. Magnetic Resonance in Medicine, 1995, 34, 402-411.	1.9	44
148	Measurement of vascular volume fraction and blood-tissue permeability constants with a pharmacokinetic model: Studies in rat muscle tumors with dynamic Gd-DTPA enhanced MRI. Magnetic Resonance in Medicine, 1994, 32, 714-724.	1.9	127
149	Susceptibility effects in porous media in the presence of flow. Journal of Magnetic Resonance Imaging, 1993, 3, 794-799.	1.9	2
150	Statistical description of microcirculatory flow as measured with an MR method. Journal of Magnetic Resonance Imaging, 1993, 3, 883-887.	1.9	5